IMPACT MECHANICS AT METEOR CRATER, ARIZONA

By

Eugene M. Shoemaker

A Dissertation Presented to the Faculty of Princeton University in Candidacy for the Degree of Doctor of Philosophy

October 1959
Princeton, New Jersey

RECOMMENDED FOR ACCEPTANCE BY THE
DEPARTMENT OF
GEOLOGY

Contents

Illustrations

Tables

Abstract

Meteor Crater is a bowl-shaped depression encompassed by a rim composed chiefly of debris stacked in layers of different composition. Original bedrock stratigraphy is preserved, inverted, in the debris. The debris rests on older disturbed strata, which are turned up at moderate to steep angles in the wall of the crater and are locally overturned near the contact with the debris. These features of Meteor Crater correspond closely to those of a crater produced by nuclear explosion where depth of burial of the device was about 1/5 the diameter of the resultant crater.

Studies of craters formed by detonation of nuclear devices show that structures of the crater rims are sensitive to the depth of explosion scaled to the yield of the device. The structure of Meteor Crater is such as would be produced by a very strong shock originating about at the level of the present crater floor, 400 feet below the original surface.

At supersonic to hypersonic velocity an impacting meteorite penetrates the ground by a complex mechanism that includes compression of the target rocks and the meteorite by shock as well as hydrodynamic flow of the compressed material under high pressure and temperature.

The depth of penetration of the meteorite, before it loses its integrity as a single body, is a function primarily of the velocity and shape of the meteorite and the densities and equations of state of the meteorite and target. The intensely compressed material then becomes dispersed in a large volume of breccia formed in the expanding shock wave.

An impact velocity of about 15 km/sec is consonant with the geology of Meteor Crater in light of the experimental equation of state of iron and inferred compressibility of the target rocks. The kinetic energy of the meteorite is estimated by scaling to have been from 1.4 to 1.7 megatons TNT equivalent.

Introduction

The origin of a crater in earth materials, produced by the sudden application of forces either from impact or explosion, has proven to be a problem peculiarly difficult to reduce to a realistic mathematical model. Solution of the mechanics of meteorite impact, however, has a direct bearing on the recognition of impact structures on the earth and on the origin of the craters of the moon.

Analysis of the formation of craters in rock by meteorite impact has followed two main lines of thought over the last 40 years. In one line, cratering by impact has been likened to cratering by chemical or nuclear explosion (Gifford, 1924 and 1930; Fairchild, 1930; Moulton, 1931, p. 305; Spencer, 1935; Wylie, 1933, 1934, and 1943; Boon, 1936; Boon and Albritton, 1936, 1937, and 1938; Baldwin, 1949; Rinehart, 1950; Gold, 1956; Hill and Gilvarry, 1956; and Gilvarry and Hill, 1956a and 1956b). In the other line of thought, developed by Öpik (1936 and 1958), La Paz (reported in Meyerhoff, 1950, and Foster, 1957), and Rostoker (1953), the problem of crater formation has been treated mainly in terms of flow of incompressible fluids, a method that has been used successfully to analyze the penetration of metal targets by very high velocity metallic jets.

In most previous papers the cratering problem has been attacked on theoretical grounds and the results then applied to Meteor Crater, Arizona. Widely discordant estimates of the mass or the energy of the meteorite are obtained from the two main methods of approach. In this paper the reasoning will be reversed. The requirements for theory will be deduced from the geology of Meteor Crater and its structural similitude with a nuclear explosion crater. A detailed analysis will then be given of how and in what form the meteoritic material reaches certain depths demanded by geological relations and how the energy is distributed during penetration.

Geology of Meteor Crater

Regional setting.--Meteor Crater lies in north-central Arizona in the Canyon Diablo region of the southern part of the Colorado Plateau (fig. 1). The climate is arid and the exposures are

---

Figure 1. Sketch geologic map of Canyon Diablo region, Arizona.

---

exceptionally good.

In the vicinity of the crater, the surface of the Plateau has very low relief and is underlain by nearly flat-lying beds of Permian and Triassic age. The crater lies near the anticlinal bend of a gentle monoclinal fold, a type of structure characteristic of this region. The strata are broken by wide-spaced northwest-trending normal faults, generally many miles in length but with only a few tens of feet to about a hundred feet of displacement. Two mutually perpendicular sets of vertical joints of uniform strike occur in the region of the crater. One set is subparallel to the normal faults and the other controls the trend of secondary stream courses (fig. 1).

Basaltic cinder cones and flows of Pleistocene and Recent age lie at distances of about 10 to 20 miles to the south, west, and northwest of the crater.

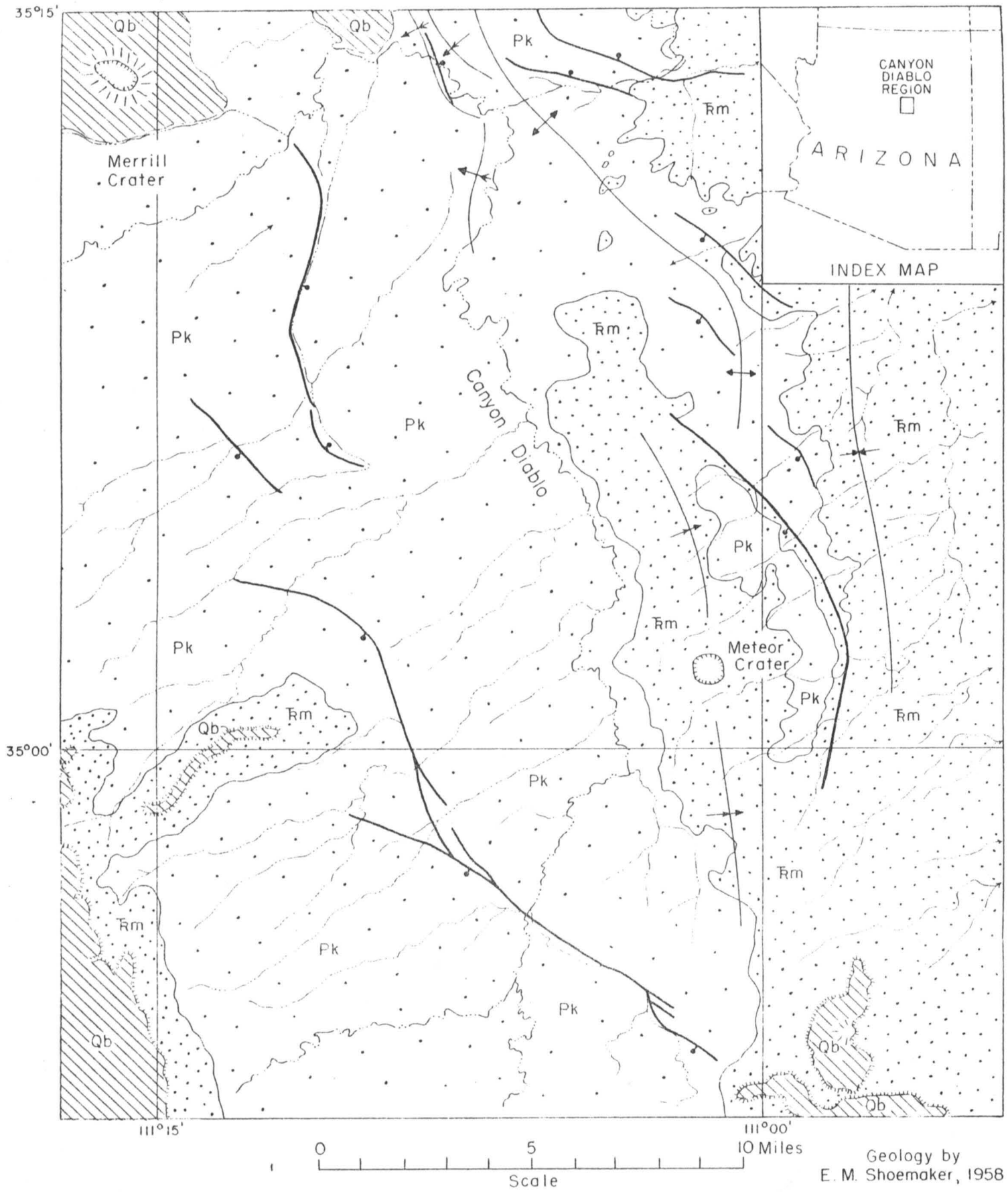

FIGURE 1.—SKETCH GEOLOGIC MAP OF CANYON DIABLO REGION, ARIZONA

Pre-Quaternary stratigraphy.--Rocks exposed at Meteor Crater range from the Coconino sandstone of Permian age to the Moenkopi formation of Triassic age. Drill holes in and around the crater have intersected the upper part of the Supai formation of Pennsylvanian and Permian age, which conformably underlies the Coconino.

The Supai formation consists of interbedded red and yellow fine-grained argillaceous sandstone and subordinate siltstone. It is more than 1,000 feet thick in this region (Peirce, 1958, p. 84), but not more than a few hundred feet have been penetrated by the drill at the crater. The Coconino sandstone (McKee, 1934) comprises about 700 to 800 feet of fine-grained saccharoidal white cross-bedded sandstone. Most of the Coconino sandstone is an unusually clean quartz sandstone; some parts contain a variable amount of calcite cement and in the lower part of the formation the quartzose sandstone is interbedded with red sandstone beds of Supai lithology. Only the upper part of the Coconino is exposed at the crater. The Coconino is overlain conformably by a 9-foot thick unit of white to yellowish- or reddish-brown, calcareous, medium- to coarse-grained sandstone referred to the Toroweap formation of Permian age (McKee, 1938).

The Kaibab formation of Permian age, which rests conformably on the Toroweap formation, comprises 265 to 270 feet of fossiliferous marine sandy dolomite, dolomitic limestone, and minor calcareous

sandstone. Three members are recognized (McKee, 1938), the lower two of which are chiefly massive dense dolomite; the upper or Alpha member is composed of well bedded limestone and dolomite with several continuous thin sandstone interbeds. The Kaibab is exposed along the steep upper part of the wall of the crater, and a large area west of Meteor Crater is essentially a stripped surface on the Alpha member (fig. 1).

In the vicinity of the crater, and to the east, beds of the Wupatki member of the Moenkopi formation (McKee, 1954) of Triassic age form a thin patchy veneer resting disconformably on the Kaibab. A 10- to 15-foot bed of pale reddish-brown, very fine grained sandstone (lower massive sandstone of McKee) lies from 1 to 3 feet above the base; the rest of the preserved part of the Wupatki member consists mainly of dark reddish-brown fissile siltstone. About 30 to 50 feet of Moenkopi strata are exposed in the wall of the crater.

Quaternary stratigraphy and structure of the crater.--Meteor Crater is a bowl-shaped depression 600 feet deep, about three-quarters of a mile in diameter, encompassed by a ridge or rim that rises 100 to 200 feet above the surrounding plain. The rim is underlain by a complex sequence of Quaternary debris and alluvium resting on disturbed Moenkopi and Kaibab strata (figs. 2 and 3).

Figure 2. Geologic map of area around Meteor Crater, Arizona.

Figure 3. Geologic map of Meteor Crater, Arizona.

The debris consists of unsorted angular fragments ranging from splinters less than a micron in size to great blocks more than 100 feet across. Because of the striking lithologic contrast among the older formations from which the debris is derived, it is possible to distinguish and map units or layers in the debris by the lithic composition and stratigraphic source of the component fragments.

The stratigraphically lowest debris unit of the rim is composed almost entirely of fragments derived from the Moenkopi formation. Within the crater this unit rests on the edge of upturned Moenkopi beds (fig. 4) or very locally grades into the Moenkopi formation;

Figure 4. Cross sections of Meteor Crater, Arizona, and nuclear explosion craters.

away from the crater wall the debris rests on the eroded surface of the Moenkopi. A unit composed of Kaibab debris rests on the Moenkopi debris. The contact is sharp where exposed within the crater, but at distances of half a mile from the crater there is slight mixing

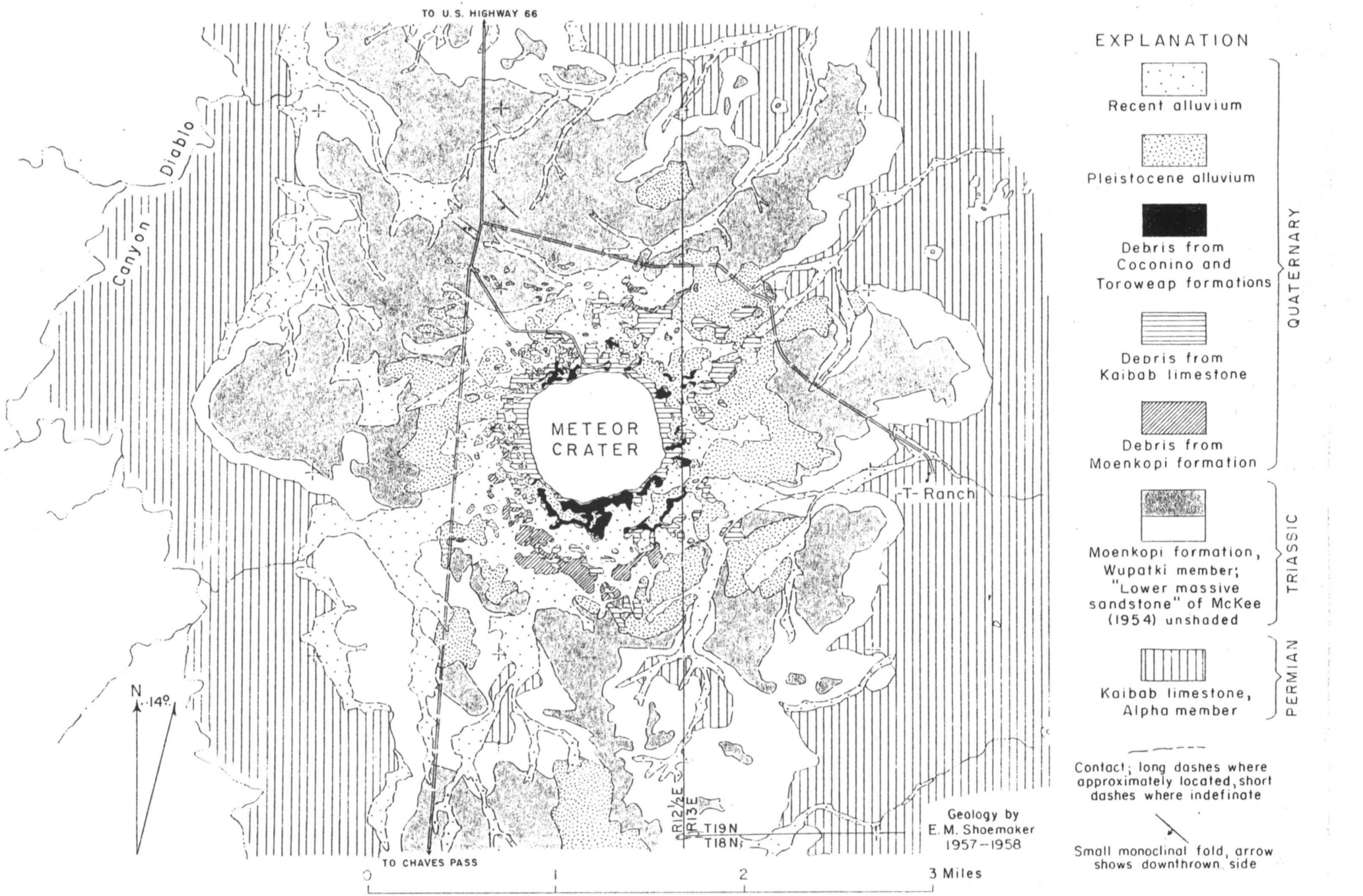

FIGURE 2.—GEOLOGIC MAP OF AREA AROUND METEOR CRATER, ARIZONA

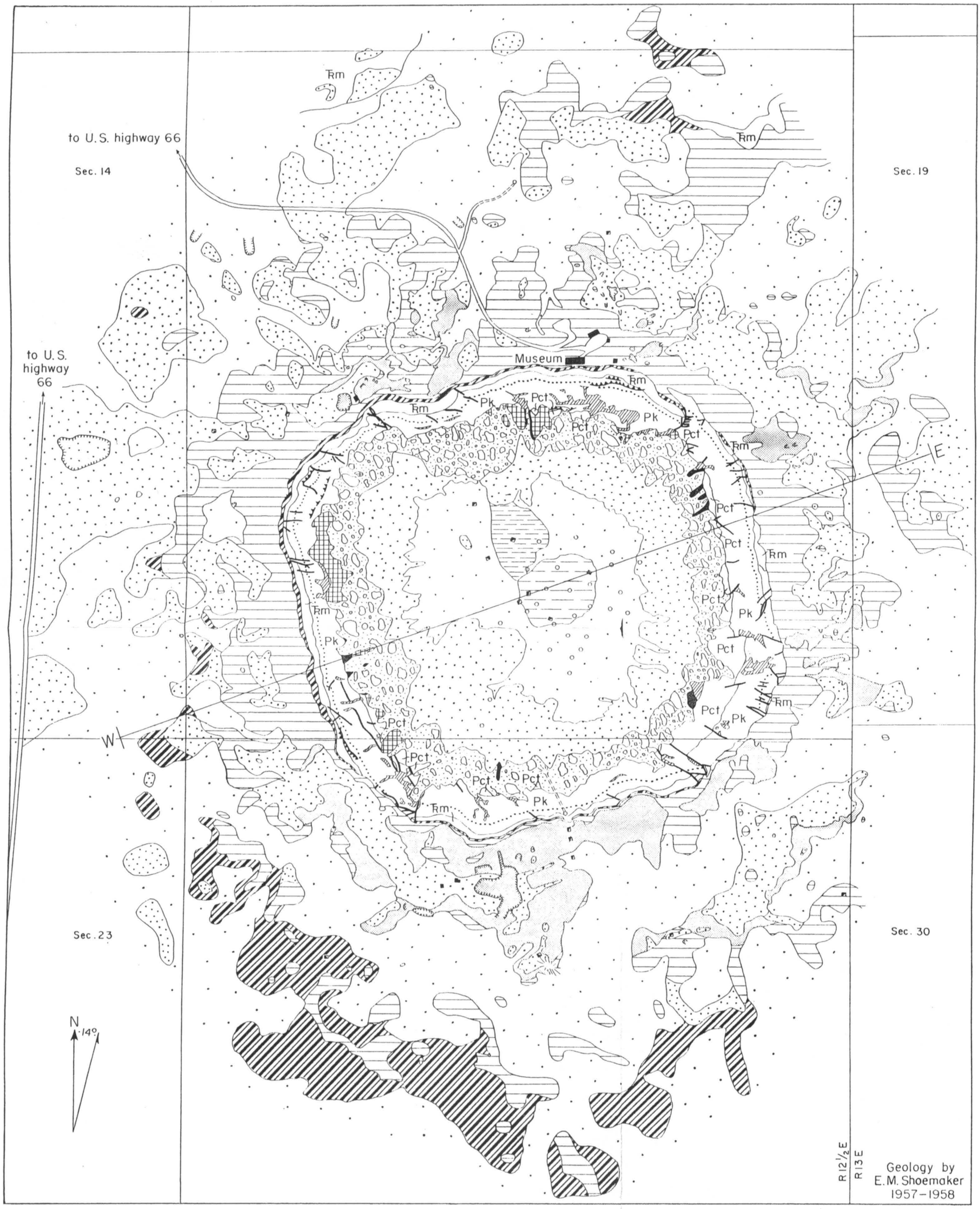

FIGURE 3.—GEOLOGIC MAP OF METEOR CRATER, ARIZONA

EXPLANATION

Recent

Alluvium

Playa beds

UNCONFORMITY

Pleistocene

Alluvium

Lake beds

Talus deposits

UNCONFORMITY

Mixed debris from Coconino, Toroweap, Kaibab, and Moenkopi formations; includes lechatelierite and meteoritic material

Debris from Coconino and Toroweap formations

Debris from Kaibab limestone

Debris from Moenkopi formation

QUATERNARY

UNCONFORMITY

Trm

Moenkopi formation

TRIASSIC

UNCONFORMITY

Pk

Kaibab limestone; dotted line is sandstone bed in Alpha member

Pct

Coconino and Toroweap formations

PERMIAN

Contact

Faults, nearly vertical or normal

Thrust fault; teeth are on side of upper plate

Authigenic breccia; fragments not mixed; occurs mostly along faults

Allogenic breccia; fragments mixed, includes lechatelierite and meteoritic material

Shaft

Adit

Pit

Dump

Drill hole

METEOR CRATER

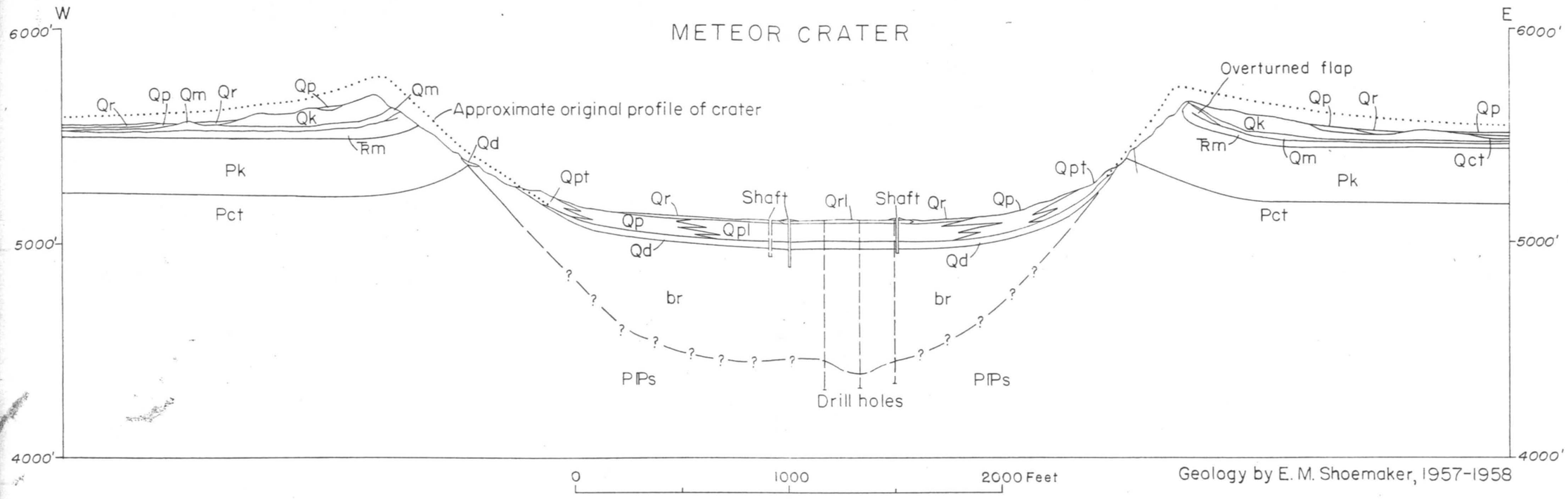

Geology by E. M. Shoemaker, 1957-1958

Qr, Recent alluvium
Qrl, Recent playa beds
Qp, Pleistocene alluvium
Qpl, Pleistocene lake beds
Qpt, Pleistocene talus

Qd, mixed debris from Coconino, Toroweap, Kaibab, and Moenkopi formations; includes lechatelierite and meteoritic material
Qct, debris from Coconino and Toroweap formations
Qk, debris from Kaibab limestone
Qm, debris from Moenkopi formation
br, breccia (includes lechatelierite and meteoritic material

Rm, Moenkopi formation (Triassic)
Pk, Kaibab limestone (Permian)
Pct, Coconino and Toroweap formations (Permian)
PPs, Supai formation (Permian and Pennsylvanian)

TEAPOT ESS CRATER

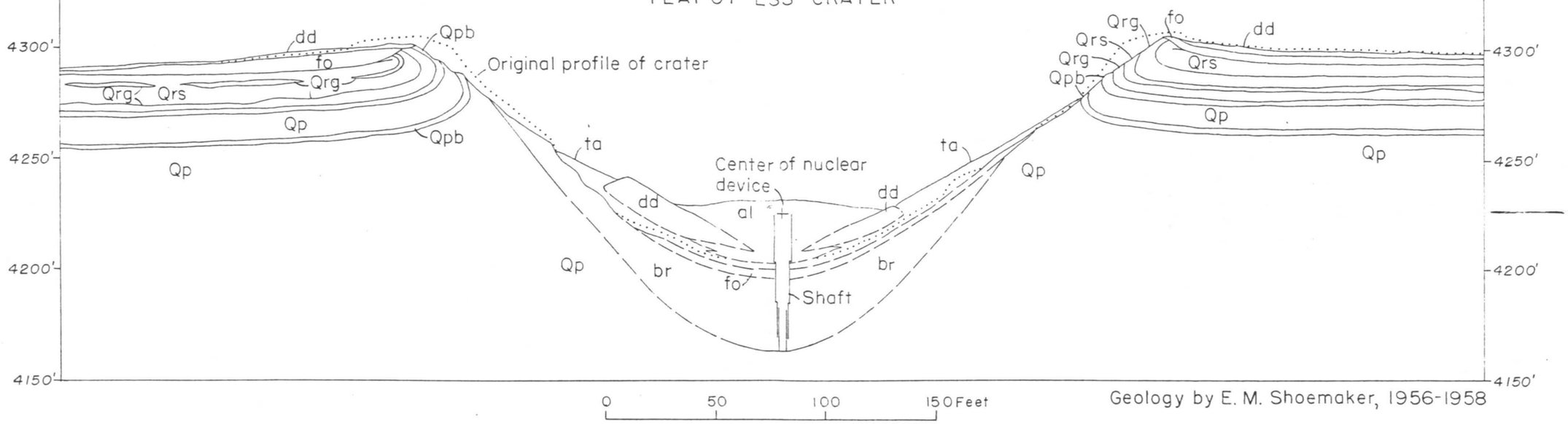

Geology by E. M. Shoemaker, 1956-1958

JANGLE U CRATER

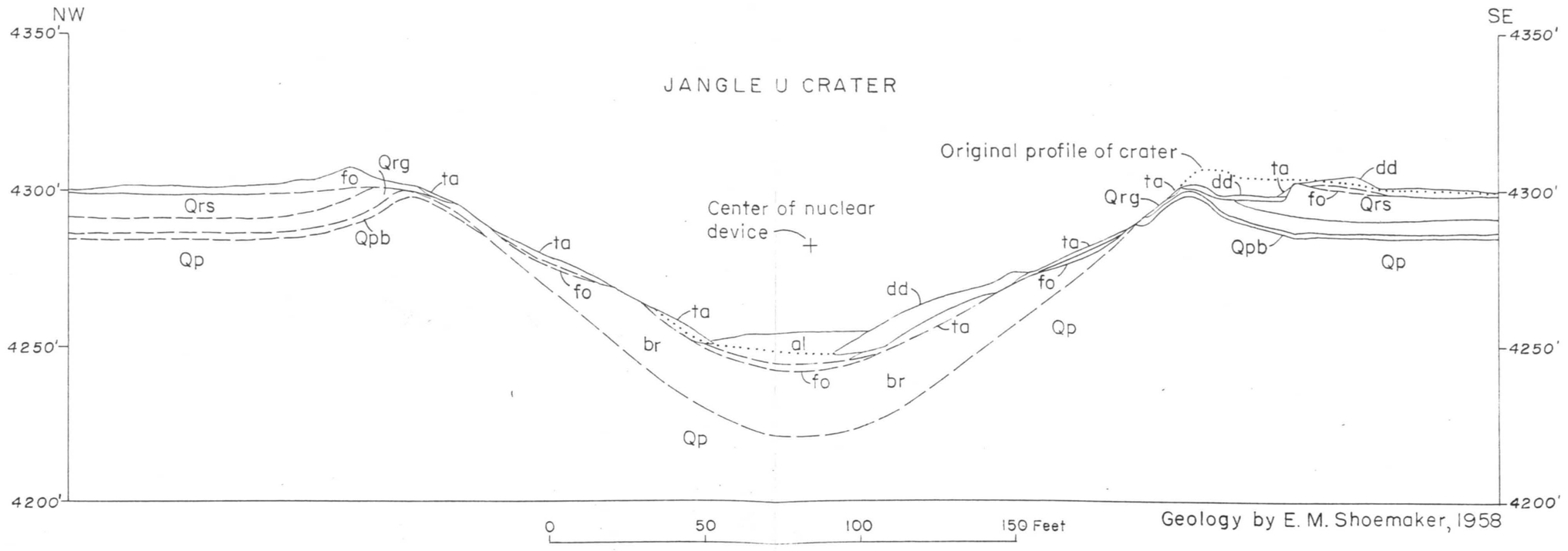

Geology by E. M. Shoemaker, 1958

dd, dump material moved by bulldozer or power shovel
ta, scree formed in crater
al, alluvium deposited in crater
fo, fallout and throwout
br, breccia

Qrs, Recent sand
Qrg, Recent gravel
Qpb, Pleistocene paleosol, B horizon
Qp, Pleistocene alluvium

of fragments at the contact. Patches of a third debris unit, composed of sandstone fragments from the Coconino and Toroweap formations, rest with sharp contact on the Kaibab debris. No fragments from the Supai formation are represented in any of the debris.

The bedrock stratigraphy is preserved, inverted, in the debris units. Not only is the gross stratigraphy preserved, but even the relative position of fragments from different beds tends to be preserved. Thus sandstone fragments from the basal sandstone bed of the Moenkopi formation occur near the top of the Moenkopi debris unit, fragments from the Alpha member of the Kaibab limestone occur at the base of the Kaibab debris unit, and brown sandstone fragments from the 9-foot thick Toroweap formation occur just above the Kaibab debris unit.

Pleistocene and Recent alluvium rests unconformably on all of the debris units as well as on bedrock. The Pleistocene alluvium forms a series of small partly dissected pediments extending out from the crater rim and also occurs as isolated patches of pediment or terrace deposits on the interstream divides. It is correlated on the basis of well developed pedocal paleosols with the Jeddito formation of Hack (1942, p. 48-54) of Pleistocene age (Leopold and Miller, 1954, p. 57-60; Shoemaker, Byers, and Roach, in press) in the Hopi Buttes region, some 50 miles to the northeast. Recent alluvium

blankets about half the area within the first half mile of the crater and extends along the floors of minor stream courses (fig. 2). It includes modern alluvium and correlatives of the Tsegi and Naha formations of Hack (1942) of Recent age (Shoemaker, Byers, and Roach, in press) in the Hopi Buttes region.

Both the Pleistocene and Recent alluvium are composed of material derived from all formations represented in the debris and also contain meteorite fragments, lechatelierite (Merrill, 1907; 1908, p. 472-478; Rogers, 1928, p. 82-84, and 1930), and other kinds of fused rock (Nininger, 1954; 1956, p. 117-134). The lechatelierite is chiefly fused Coconino sandstone. Oxidized meteoritic material and lechatelierite are locally abundant in the Pleistocene alluvium where it occurs fairly high on the crater rim. Unoxidized meteoritic material occurs in two principal forms, 1) large crystalline fragments composed mainly of two nickel-iron minerals, kamacite and taenite (Merrill and Tassin, 1907), and 2) minute spherical particles of nickel-iron (Tilghman, 1905, p. 898-899, 907; Nininger, 1949, 1951a, 1951b, p. 80-81). The bulk of the meteoritic material distributed about the crater is apparently in the form of small particles. The total quantity of fine-grained meteoritic debris about the crater, which occurs not only in the Pleistocene and Recent alluvium, but also as lag and dispersed in colluvium, has been estimated by Rinehart (1958, p. 150) as about 12,000 tons.

Beds ranging from the Coconino sandstone to the Moenkopi formation are exposed in the crater walls. Low in the crater the beds dip gently outward. The dips are generally steeper close to the contact with the debris on the rim, and beds are overturned along various stretches totalling about one-third of the perimeter of the crater. Along the north and east walls of the crater the Moenkopi locally can be seen to be folded back on itself, the upper limb of the fold consisting of a flap that has been rotated in places more than 180° away from the crater (fig. 4). At one place in the southeast corner of the crater the flap grades outward into disaggregated debris, but in most places there is a distinct break between the debris and the coherent flap.

Rocks now represented by the debris of the rim have been peeled back from the area of the crater somewhat like the petals of a flower blossoming. The axial plane of the fold in three dimensions is a flat cone, with apex downward and concentric with the crater, that intersects the crater wall. If eroded parts of the wall were restored, more overturned beds would be exposed.

The upturned and overturned strata are broken or torn by a number of small nearly vertical faults with scissors type of displacement. A majority of these tears are parallel with the northwesterly regional joint set and a subordinate number are parallel with the northeasterly set. Regional jointing has controlled the shape of the crater, which

is somewhat squarish in outline; the diagonals of the "square" coincide with the trend of the two main sets of joints. The largest tears occur in the "corners" of the crater. In the northeast corner of the crater a torn end of the overturned flap of the east wall forms a projection suspended in debris. A few normal faults, concentric with the crater wall, occur on the southwest side. There are also a number of small thrust faults on the north and west sides of the crater. Relative displacement of the lower plate is invariably away from the center of the crater. Crushed rock is locally present along all types of faults; it has been designated authigenic breccia on figure 3 to distinguish it from another type of breccia under the crater floor.

The floor of the crater is underlain by Quaternary strata, debris, and breccia. Pleistocene talus mantles the lowest parts of the crater walls and grades into Pleistocene alluvium along the floor. The Pleistocene alluvium in turn interfingers with a series of lake beds about 100 feet thick toward the center of the crater. Several feet of Recent alluvium and playa beds rest unconformably on the Pleistocene. Where exposed in shafts, the lowermost Pleistocene lake beds contain chunks of pumiceous frothy lechatelierite.

A layer of mixed debris underlies the Pleistocene talus and lake beds and rests on bedrock and on breccia. This layer is composed of fragments derived from all formations intersected by the crater and

includes much fused and partially fused rock and oxidized meteoritic material. The material from all the different sources is thoroughly mixed. Where intersected by a shaft in the crater floor, it is about 30 feet thick and almost perfectly massive, but exhibits a distinct grading from coarse to fine going from base to top. The average grain size, about half an inch, is much less than in the debris units of the rim or in the underlying breccia, the coarsest fragments at the base rarely exceeding 1 foot in diameter. I believe this unit was formed by fall-out of debris thrown to great height. It has not been recognized outside of the crater, probably because it has been entirely eroded away. Its constituents have been partly redeposited in the Pleistocene and Recent alluvium.

Where exposed at the surface, the breccia underlying the mixed debris is composed chiefly of large blocks of Kaibab, but where exposed in shafts under the central crater floor, the breccia is made up chiefly of shattered and twisted blocks of Coconino. Extensive drilling conducted by Barringer (1905, 1910, 1914) and his associates (Tilghman, 1905) has shown that at several hundred feet depth much finely crushed sandstone and some fused and partially fused rock and meteoritic material is present. Some drill cuttings from about 600 feet depth contain fairly abundant meteoritic material. In cuttings examined by the writer the meteoritic material is chiefly

in the form of fine particles dispersed in glass similar to the impactite described by Nininger (1954) and by Spencer (1933, p. 394-399) from the Wabar and Henbury meteorite craters. Cores of ordinary siltstone and sandstone of the Supai were obtained at depths of 700 feet and deeper. The lateral dimensions of the breccia are not known because the drilling was concentrated in the center of the crater. Some of the meteorite-bearing or allogenic breccia was evidently encountered in a hole drilled from 1920 to 1922 on the south rim of the crater (Barringer, 1924). (See log of hole in Hager, 1953, p. 840-841.)

Mechanism of crater formation

Teapot Ess crater.--Nearly all the major structural features of Meteor Crater, Arizona, are reproduced in a crater in the alluvium of Yucca Flat, Nevada, formed by underground explosion of a nuclear device. The Teapot Ess crater (fig. 4), about 300 feet across and originally about 100 feet deep, was produced in 1955 by a 1.2 kiloton device detonated at a depth of 67 feet below the surface (Johnson, 1959, p. 10). Beds of alluvium exposed in the rim are peeled back in an overturned syncline just as the bedrock is peeled back at Meteor Crater. The upper limb of the fold is overlain and locally passes outward into debris that roughly preserves, inverted, the original alluvial stratigraphy. Glass is present in the uppermost part of the debris. A thin layer of debris formed by fallout or fall back is also present in the crater. The floor and lower walls of the crater are underlain by a thick lens of breccia containing mixed fragments of alluvium and dispersed glass. Some of the fragments are strongly sheared and compressed. The glass is composed of alluvium that was fused or partially fused by shock. The breccia was formed by complex movement of material within the crater; locally the original bedding of the alluvium is roughly preserved in the breccia.

Formation of craters by nuclear explosion.--A crater with the structure of Teapot Ess crater is formed chiefly by two mechanisms,

which operate in succession (fig. 7, sketches 6-9). First the alluvium, as it is engulfed by a compressional shock caused by the explosion, is accelerated in all directions radially outward from the detonated device, and an expanding cavity is formed underground. When the shock reaches the free surface of the ground it is reflected as a tensional wave. Momentum is trapped in the material above the cavity and it continues to move up and outward, individual fragments following ballistic trajectories. Some kinetic energy may also be imparted to the fragments from expanding gases in the cavity. Ejected fragments close to the crater maintain their approximate relative positions, inverted during flight. Along low trajectories, their range is largely a function of the angle at which they are thrown out, which in turn varies continuously with their original position relative to the nuclear device. The margin of the crater is determined primarily by the radial distance, in plan, at which the reflected tensional wave is just strong enough to lift and separate the alluvium. The position at which this occurs is just inside of and concentric with the hinge of the overturned flap, i.e. the intersection of the axial plane of overturning with the surface of the ground. The reflected tensional wave starts a fracture at the surface but does not appreciably change the momentum of most of the material thrown out. Beds are sheared off along a roughly conical surface that starts at

the surface slightly inside the hinge and is propagated downward to join tangentially the lower part of the hole expanded behind the shock front. Material brecciated by very strong shock initially has the form of a roughly spherical shell around the hole, but most of the upper hemisphere is thrown out and the lower hemisphere is sheared out in the form of a concavo-convex lens. Overturning of the beds in the upper crater wall may be looked on as drag along the conical shear zone.

It is essential that the shock originate deeper than a certain minimum distance below the surface, relative to the total energy released, in order to produce the overturned syncline in the rim. A crater formed near the Teapot Ess crater by a nuclear device of the same yield, but detonated at 18 feet depth rather than 67 feet (fig. 4, Jangle U crater), has an anticline under the rim, not a syncline. An explosion at a depth this shallow (relative to the yield of the device) produces a crater more through radial expansion of the hole behind the shock and less by ejection of material than in the case of Teapot Ess crater. Greatest expansion of the hole occurs at the surface because of upward relief of stress at the free surface, which manifests itself in concentric anticlinal buckling.

Shock and apparent origin of shock at Meteor Crater.--The fact that rock was fused, in particular that some relatively pure quartzose

sandstone was fused, suggests by itself that shock was involved in the origin of Meteor Crater, as the melting point of quartz is considerably above ordinary magmatic temperatures. The structures are such as would be produced by a very strong shock originating about at the level of the present crater floor 400 feet below the original surface. A minimum scaled depth of penetration of the meteorite or of a major part of the energy associated with the meteorite is indicated by the overturned synclinal structure of the rim. As will be shown, a closer estimate of the depth for the apparent origin of the shock can be obtained from the base of the breccia under the crater floor by scaling from Teapot Ess crater. Some limits may also be set on the mechanics of impact by the fact that the shock was strong enough to fuse Coconino sandstone, at a depth of some 300 feet or more below the surface, and that part of the meteorite itself was apparently fused by shock on impact, as shown by the dispersal of spherical meteorite particles in some of the fused rock.

Not all meteorite craters exhibit overturned synclines in the rim, as at Meteor Crater, Arizona, which indicates that the scaled depth of penetration on impact is not always as great. The rim of the main meteorite crater at Odessa, Texas, for example, is underlain by an anticline similar to that of the Jangle U crater (compare with Hardy, 1953; Sellards and Evans, 1941). It may be noted that no crater of

demonstrated volcanic origin, particularly the maar type of crater with which Meteor Crater has been compared (Gilbert, 1896, p. 11; Darton, 1916, 1945), has a structure or arrangement of debris in the rim comparable to that at Meteor Crater (compare with Shoemaker, 1957). The mechanics of typical maars or diatremes lead to collapse of material from the crater walls into the vent, generally leaving the surrounding country rock undisturbed (Shoemaker, 1956; Shoemaker and Moore, 1956; Shoemaker, Byers, and Roach, in press).

Penetration of meteorite

We may now proceed to inquire how the meteoritic material and energy were delivered to the depths indicated at Meteor Crater. At sufficiently high impact velocity a meteorite will penetrate the ground by a complex mechanism which may be described in terms of three phenomena, 1) compression of the target rocks and meteorite by shock, 2) hydrodynamic flow of the compressed material, and 3) dispersal of the meteoritic material in the flowing mass, which may be loosely referred to as the shock wave (Courant and Friedrichs, 1948, p. 119). These phenomena occur simultaneously or overlap each other in time, but their relative importance changes during the course of the penetration process. For purposes of discussion they will be treated separately in the order in which they successively become the dominant factor during penetration.

Compression by shock.--Consider first the hypothetical case of two semi-infinite bodies colliding along a plane interface, moving in relation to each other at speeds exceeding the acoustic velocity of either material and in a direction perpendicular to the interface. A plane shock will be propagated from the interface into both colliding bodies. For most practical as well as theoretical purposes the shock front may be considered a zone of infinitesimal width across which there is a discontinuous jump of pressure and velocity of the medium

(particle velocity). The following relations have been derived for the changes across the shock front, propagated into a body at rest, from the laws of conservation of mass, momentum, and energy--the Rankine-Hugoniot conditions (Courant and Friedrichs, 1948, p. 121-126),

$$U\rho_0 = (U - \mu)\rho \qquad \text{(conservation of mass)}, \qquad (1)$$

$$\rho_0 U\mu = P \qquad \text{(conservation of momentum)}, \qquad (2)$$

$$E = \frac{P}{2}(1/\rho_0 - 1/\rho) \qquad \text{(conservation of energy)}, \qquad (3)$$

where U = shock velocity, μ = particle velocity behind shock front, ρ_0 = initial density, ρ = density behind shock front, P = change of pressure across shock front, and E = change of internal energy across the shock front. These conditions are rigorous and independent of the width of the shock front.

Two further rigorous conditions connect the shocks in the two bodies. First, because of the continuity of the two bodies across the collision interface, the particle velocity between the shock fronts must be the same. Secondly, from the law of equality of action and reaction, the pressure between the shock fronts must be the same. This may be most easily visualized, perhaps, if viewed from coordinates fixed with reference to the interface (Gallilean transformation). Here the particle velocity between the shocks reduces to zero on either side of the interface and the shock velocities must be such as to conserve momentum. It may be seen that, in homogeneous media, the shock velocities will remain constant.

Relative positions of shocks and collision interface of two homogeneous semi-infinite colliding bodies (meteorite and ground) at unit interval of time after collision

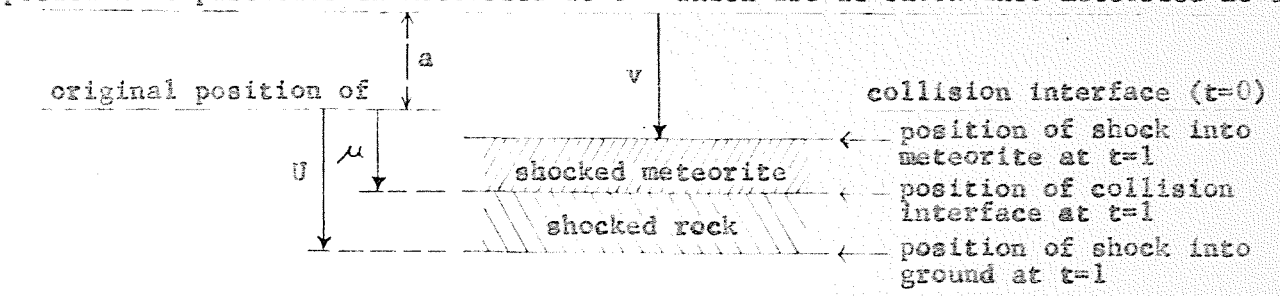

t = Interval of time

a = Initial thickness of meteorite engulfed by shock in unit interval of time

v = Initial velocity of meteorite relative to unshocked ground

U = Shock velocity into ground relative to unshocked ground

μ = Particle velocity of shocked target rocks relative to unshocked ground (identical with velocity of collision interface relative to unshocked ground)

$V_{xo} = U =$ Initial volume of rock per unit area of shock front engulfed by shock in unit interval of time

V_x = Volume of shocked rock per unit area of shock front at unit interval of time

ρ_{xo} = Initial density of rock

ρ_x = Density of shocked rock

$\delta_x = \frac{V_{xo} - V_x}{V_{xo}} = \frac{\rho_x - \rho_{xo}}{\rho_x}$ = Compression of rock

$V_{mo} = a =$ Initial volume of meteorite per unit area of shock front engulfed by shock in unit interval of time

V_m = Volume of shocked meteorite per unit area of shock front at unit interval of time

ρ_{mo} = Initial density of meteorite

ρ_m = Density of shocked meteorite

$m = \rho_{mo} V_{mo} =$ Mass of meteorite engulfed by shock in unit interval of time per unit area of shock

$\delta_m = \frac{V_{mo} - V_m}{V_{mo}} = \frac{\rho_m - \rho_{mo}}{\rho_m}$ = Compression of meteorite

$x = \rho_{xo} V_{xo} =$ Mass of rock engulfed by shock in unit interval of time per unit area of shock

Referring all motion to a system of reference which takes one body (the ground) at rest, the following relations may be derived (see sketch for definition of symbols):

$$\delta_m = \frac{V_{mo} - (V_{mo} + \mu - v)}{V_{mo}} = \frac{v - \mu}{V_{mo}}, \qquad V_{mo} = \frac{v - \mu}{\delta_m} \tag{4}$$

$$\delta_x = \frac{U - (U - \mu)}{U} = \frac{\mu}{U} = \frac{\mu}{V_{xo}}, \qquad V_{xo} = \frac{\mu}{\delta_x}. \tag{5}$$

From conservation of momentum,

$$mv = \mu(m + x), \qquad \frac{m(v - \mu)}{\mu} = x \tag{6}$$

$$m = V_{mo}\rho_{mo} = \frac{(v - \mu)\rho_{mo}}{\delta_m} \qquad \text{(substitute 4)} \tag{7}$$

$$x = V_{xo}\rho_{xo} = \frac{\mu\rho_{xo}}{\delta_x} \qquad \text{(substitute 5)} \tag{8}$$

Combining (6), (7), and (8)

$$\frac{(v - \mu)\rho_{mo}(v - \mu)}{\mu\delta_m} = \frac{\mu\rho_{xo}}{\delta_x}, \qquad (v - \mu)^2 = \frac{\mu^2\rho_{xo}\delta_m}{\rho_{mo}\delta_x}, \tag{9}$$

$$v = \mu\left(1 \pm \sqrt{\frac{\rho_{xo}\delta_m}{\rho_{mo}\delta_x}}\right), \tag{10}$$

and, as μ cannot exceed v under compression we are concerned only with the positive root. Employing equations (5) and (2) we may also write

$$\mu = \frac{v}{1 + \sqrt{\frac{\rho_{xo}\delta_m}{\rho_{mo}\delta_x}}}, \qquad U = \frac{v}{\delta_x\left(1 + \sqrt{\frac{\rho_{xo}\delta_m}{\rho_{mo}\delta_x}}\right)}, \tag{11}$$

and

$$P = \left[\frac{v}{\sqrt{\frac{\delta_x}{\rho_{xo}}} + \sqrt{\frac{\delta_m}{\rho_{mo}}}}\right]^2. \tag{12}$$

The particle velocity or rate of penetration of the moving body (meteorite) into ground by compression, μ, the velocity of the shock into the ground, U, and the pressure, P, are thus functions of the velocity of the meteorite, v, the initial densities of the meteorite and target, ρ_{mo} and ρ_{xo}, and the compression by shock of the meteorite and target δ_m and δ_x. From the form of equations 11, it may be seen that shocks may also be generated by impact at velocities less than the acoustic velocities of the colliding bodies, but the initial pressure and compression of the meteorite and target rocks will be less than in the cases considered here. The initial densities may be considered known; what is required for solution of (11) and (12) is a knowledge of one of the variables μ, U, v, or P, and the equations of state, or more specifically, the hugoniot curves (the relations between pressure and specific volume or density under shock conditions), for the meteorite and the rocks.

The hugoniot for iron has recently been determined by impact using relations of the type derived above (Altshuler and others, 1958), up to

4.5 megabars. Canyon Diablo meteorites average about 94 percent iron and 5 percent nickel. Some unusual compression has been observed for alloys of 30 percent nickel at low pressure (Bridgman, 1949, p. 215-216), but the error will probably be minor in treating the meteorite as pure iron in the pressure ranges of interest. Employing the condition that

$$P = \rho_{xo} \mu U = \rho_{mo} \mu_m U_m , \tag{13}$$

it may be shown by substitution that

$$v = \mu_m \left(1 + \sqrt{\frac{\rho_{mo} \delta_x}{\rho_{xo} \delta_m}} \right) = \delta_m U_m \left(1 + \sqrt{\frac{\rho_{mo} \delta_x}{\rho_{xo} \delta_m}} \right), \tag{14}$$

where μ_m is particle velocity in the meteorite behind the shock and U_m is the shock velocity in the meteorite, both relative to unshocked meteorite. The relation between the experimentally determined velocities for iron is linear, within experimental error, over the pressure range investigated, and is given (Altshuler and others, 1958, p. 881) by

$$U_m = 3.80 + 1.58 \mu_m , \tag{15}$$

where U_m and μ_m are measured in kilometers per second. Combining (14) and (15), compression of the rock may be written as a function of the velocity of the meteorite and compression of the meteorite

$$\delta_x = \frac{\rho_{xo}}{(3.80)^2 \rho_{mo} \delta_m} \left[v - \delta_m (1.58\, v + 3.80) \right]^2 . \tag{16}$$

Taking $\rho_{xo}/\rho_{mo} = 1/3$, the loci of solutions for values of v = 10, 15, and 20 km/sec. are shown in figure 5, where δ_x is plotted as a

---

Figure 5. Compression of rocks at Meteor Crater, Arizona, as a function of compression of the meteorite and of pressure.

---

function of δ_m and corresponding experimental values of pressure. Solutions for v = 20 km/sec. are based on (15) but are above the experimental range of pressure.

It remains now to assess the probable hugoniot for the target rocks in order to reduce the problem to a single unknown, the impact velocity, v. The problem of compression of rocks under high pressure has been widely discussed in connection with the internal constitution of the earth (Bullen, 1946, 1949, 1950, 1952, 1956; Ramsey, 1948; Elsasser, 1951; Birch 1952; Verhoogen, 1953; and Knopoff and Uffen, 1954). No experimental data exists for pressures in the principal range of interest, except the reasonably well defined density versus depth or pressure curves of the earth itself (Bullen, 1940, 1942, and 1950). Nearly all published experimental data pertinent to the problem are plotted in figure 6 in coordinates of density and pressure. Bridgman

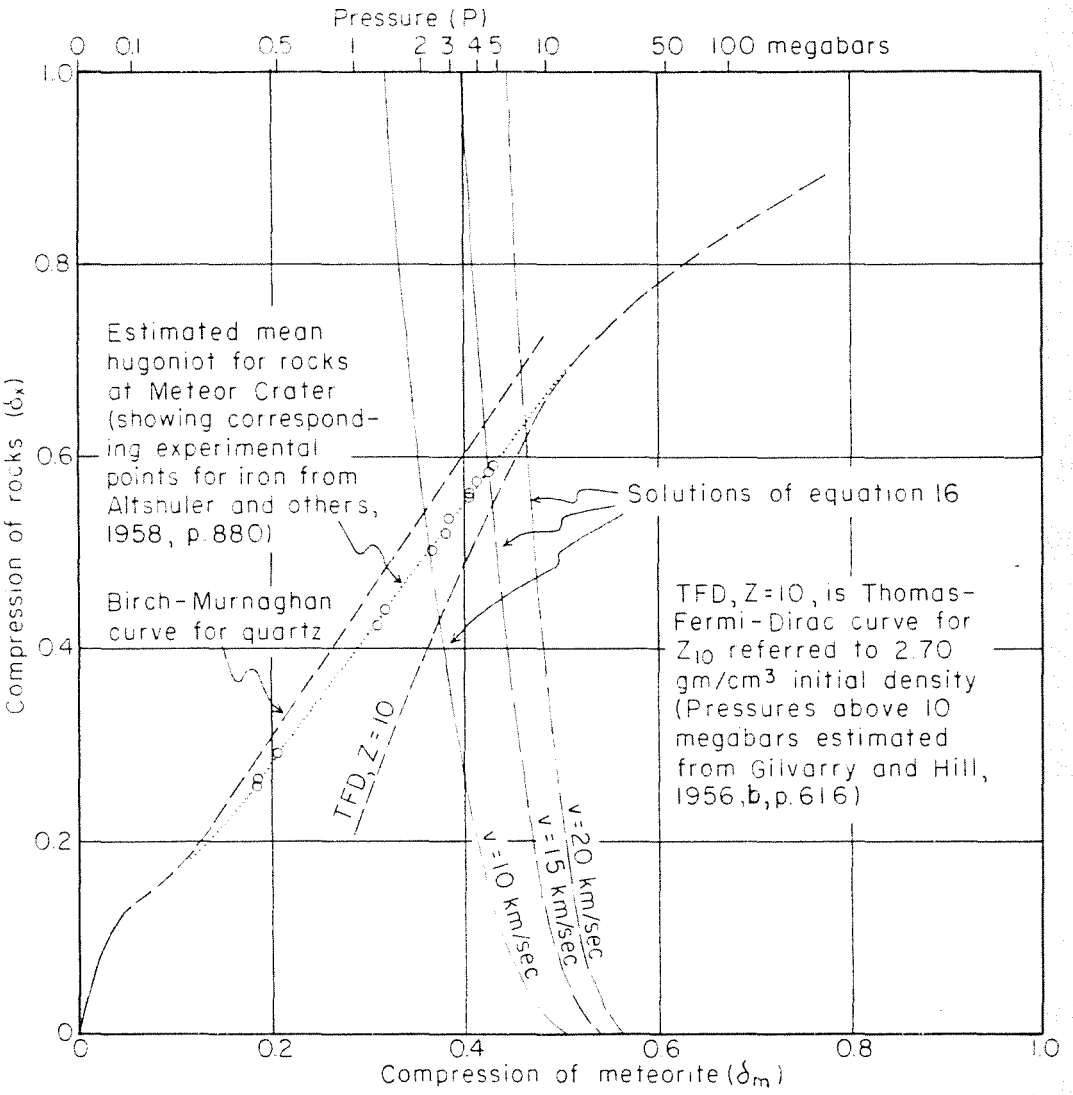

FIGURE 5.—COMPRESSION OF ROCKS AT METEOR CRATER, ARIZONA AS A FUNCTION OF COMPRESSION OF THE METEORITE AND OF PRESSURE.

Figure 6. Density-pressure curves for iron, rocks, and rock-forming minerals.

(1928, 1939, 1948a, and 1948b) has obtained the compression of quartz to 100,000 bars, of calcite to 50,000 bars, and of olivine and a few other silicate minerals to 40,000 bars. The hugoniot curves for two types of gabbro and a dunite have recently been obtained up to about 0.7 megabars (Hughes and McQueen, 1958) by shock techniques.

Density versus pressure curves for the minerals in question have been computed from the Birch-Murnaghan equation (fig. 6), based on the theory of elastic strain (Murnaghan, 1937; Birch, 1947; 1952, p. 241),

$$P = \frac{3}{2}\beta_0 \left[(\rho/\rho_0)^{7/3} - (\rho/\rho_0)^{5/3}\right] \left\{1 - \xi\left[(\rho/\rho_0)^{2/3} - 1\right] + \ldots\right\}, \quad (17)$$

where β_0 is the initial compressibility, taking $\xi = 0$, and using Bridgman's data for initial compressibility. This equation fits Bridgman's data satisfactorily, in the absence of polymorphic transitions, except for quartz. For quartz the compressibility to 100,000 bars was used, in order to extend the curve smoothly from the experimental data. A curve for dolomite was drawn from a single determination of compressibility by Madelung and Fuchs (1921, p. 306).

It may be seen that the curve for iron computed by Birch (1952, p. 278), reduced to 7.85 initial density, represents the experimental hugoniot fairly well up to about 2 megabars. The principal departures below 2 megabars are due to polymorphic transformation (Bancroft, Peterson, and Minshall, 1956). The principal departure of the experimental hugoniot for dunite from the Birch-Murnaghan curve for olivine may also be due to a polymorphic transformation; polymorphism has been indicated as the cause for a similar hump in the hugoniot for gabbros (Hughes and McQueen, 1958, p. 964-965). The deviations below 1 megabar known to be due to polymorphism are probably about of the order to be expected for other silicates, quartz, and carbonates. At low pressure the specific volumes of these rock-forming minerals are largely governed by the ionic radius of oxygen and their density may be expected to behave in the same general way under pressure.

At pressures around 10 megabars and higher the densities of most substances may be expected to approach that given by the Thomas-Fermi-Dirac quantum statistical model of the atom (Slater and Krutter, 1935; Feynman, Metropolis, and Teller, 1949; March, 1957). Curves for iron and for atomic number, $Z = 10$, have been drawn from solutions of the Thomas-Fermi-Dirac equation at 0 degrees Kelvin for $Z = 26$

EXPLANATION

Experimentally determined hugoniot curve (density–pressure curve for shock conditions), showing location of experimental points

Theoretical density–pressure curve (isothermal), showing location of calculated points

Density–pressure curve of the earth, calculated from seismic data, the mean density, and the moment of inertia of the earth

Estimated mean hogoniot curve for rocks at Meteor Crater, Arizona, derived by interpolation between theoretical curves

Sources of data on hugoniot for iron

(1) Bridgman (1949, p.198)
(2) Goranson and others (1955, p.1477)
(3) Bancroft, Peterson, and Minshall (1956, p.294)
(4) Walsh and others (1957, p.198)
(5) Altshuler and others (1958, p.880)

HUGONIOT FOR IRON

BIRCH-MURNAGHAN CURVE FOR IRON after Birch (1952, p.278)

MODEL B (Bullen, 1950, p.58)

MODEL A (Bullen, 1942, p.27)

THOMAS-FERMI-DIRAC CURVE FOR IRON

BIRCH-MURNAGHAN CURVE FOR QUARTZ

ESTIMATED MEAN HUGONIOT FOR ROCKS AT METEOR CRATER

THOMAS-FERMI-DIRAC CURVE FOR Z=10

DENSITY OF THE EARTH MODEL A (Bullen, 1940, p.246)

HUGONIOT FOR SAN MARCOS GABBRO (Hughes and McQueen, 1958, p.963)

HUGONIOT FOR JACKSON CO. DUNITE (Hughes and McQueen, 1958, p.963)

DENSITY OF THE EARTH MODEL B (Bullen, 1950, p.58)

HUGONIOT FOR OLIVINE (Bridgman, 1948b, p.78)

BIRCH-MURNAGHAN CURVE FOR OLIVINE

BIRCH-MURNAGHAN CURVE FOR DOLOMITE

BIRCH-MURNAGHAN CURVE FOR CALCITE

HUGONIOT FOR CALCITE (Bridgman, 1939, p.9)

HUGONIOT FOR QUARTZ (Bridgman, 1928, p.294; 1948a, p.68)

BIRCH-MURNAGHAN EQUATION

$$P = \frac{3}{2B_0}\left[\left(\frac{\rho}{\rho_0}\right)^{7/3} - \left(\frac{\rho}{\rho_0}\right)^{5/3}\right]\left\{1 - \xi\left[\left(\frac{\rho}{\rho_0}\right)^{2/3} - 1\right] + \ldots\right\}$$

Values adopted for parameters of equation

	ρ_0(gm/cm)	B_0(1/megabars)	ξ
iron	7.85	0.594	0
olivine	3.32	0.810	0
dolomite	2.87_3	1.21	0
calcite	2.71_1	1.341	0
quartz	2.65_4	1.88	0

THOMAS-FERMI-DIRAC EQUATION

$$d^2\psi/dx^2 = x(\epsilon + \psi^{1/2}/x^{1/2})^3$$

$$P = \frac{Z^2e^2}{4\pi\mu^4}\left[\left(\psi_{(x_0)}/x_0\right)^{1/2} + \epsilon\right]^5 \left\{1 - \frac{5\epsilon/4}{\left(\psi_{(x_0)}/x_0\right)^{1/2} + \epsilon}\right\}$$

$$\mu = a_0(9\pi^2/128Z)^{1/3}, \quad \epsilon = (3/32\pi^2)^{1/3}Z^{-2/3}$$

$$\rho = \frac{3 \text{ atomic weight}}{4\pi(\mu x_0)^3 N}$$

Values adopted for parameters of equation

$e = 4.8022 \times 10^{-10}$ e.s.u.
$a_0 = 5.2915 \times 10^{-9}$ cm
$N = 6.0254 \times 10^{23}$ gm/mol
} DuMond and Cohen (1952, p.457)

atomic weight of iron (Z_{26}) = 55.85
atomic weight of $Z_{10} = 2Z$

Solution of Thomas-Fermi-Dirac equation for $\psi_{(x_0)}$ and x_0 from Metropolis and Reitz (1951, p.556-59)

Density (ρ) (gm/cm)

Pressure (P)

$\times 10^{-2}$ megabars

$\times 10^{-1}$ megabars

megabars

FIGURE 6.— DENSITY–PRESSURE CURVES FOR IRON, ROCKS, AND ROCK-FORMING MINERALS

and 10 by Metropolis and Reitz (1951). The mean atomic number of quartz, calcite, and forsterite is 10.0 and of dolomite, 9.2. Knopoff and Uffen have shown that the effective mean atomic number, obtained by averaging by specific atomic volume, is slightly greater than the mean averaged by number of atoms, but the use of their refined mean is offset by error in the interpolative procedure by which their curves are derived.

An estimated mean hugoniot curve has been drawn (fig. 6) for the rocks at Meteor Crater by interpolation between the Birch-Murnaghan curves for quartz, calcite, and dolomite and the Thomas-Fermi-Dirac curve for Z = 10. The curve, as drawn, may be subject to an error of 10 to 20 percent or more in the range of 1 to 10 megabars. The chief potential sources of error are polymorphism, at around 1 megabar, and the thermal component of pressure, at around 10 megabars. These sources of error tend to be compensating. No account has been taken of the initial porosity of the rocks, which probably averages less than 15 percent (see Jakosky, Wilson, and Daly, 1932, p. 23). The error in total compression, due to neglect of initial porosity, will be compensated to a considerable extent by an additional thermal component of pressure in the range of 1 to 10 megabars (compare with Altshuler and others, 1958, p. 881-883).

A curve for compression of the rocks at Meteor Crater as a function of the compression of the meteorite has been drawn (dotted line in fig. 5) from the estimated mean hugoniot of the rocks and the experimental hugoniot for iron shown in figure 6. The intersection of this curve (fig. 5) with solutions of equation 16 gives corresponding values for compression of the rocks and of the meteorite for specified values of impact velocity and permits solutions of equations 11, 12, and 14 (table 1). A 10 percent error in the estimated mean hugoniot of the rocks, which would include all points enclosed by the Birch-Murnaghan and Thomas-Fermi-Dirac curves and the solutions of equation 16 for 10 and 20 km/sec. on figure 5, would introduce an error of about 5 percent for the quantity $\frac{x}{m}$ in table 1. Corresponding errors in the computed values for μ, U_m, and μ_m range from 3 to 5 percent, for U up to about 7 percent, and for P up to about 8 percent.

An estimate of the minimum possible impact velocity may now be made from the fact that part of the meteorite was fused by shock. Fusion will occur when the thermal component of internal energy reaches the enthalpy required for fusion under shock conditions. Adopting a melting point for iron of 2,460 C at 2 megabars pressure (Strong, 1959, p. 657-658), a mean heat capacity of 0.6 joules/gm/°C, and a latent heat of fusion of 270 joules/gm, the enthalpy required for fusion is about 1,700 joules. As shown by the data of Altshuler and others (1958, p. 880-883), the

Table 1.--Solutions of equations 11, 12, and 14 for adopted values of ρ_{xo} = 2.62 gm/cm, ρ_{mo} = 7.85 gm/cm

v =	10 km/sec.	15 km/sec.	20 km/sec.
δ_m (from fig. 5) =	0.36_5	0.42_6	0.46_3
δ_x (from fig. 5) =	0.50_3	0.58_4	0.63_3
$\frac{x}{m} = \sqrt{\frac{\rho_{xo}\,\delta_m}{\rho_{mo}\,\delta_x}}$ =	0.49_2	0.49_3	0.49_3
μ =	6.7_0 km/sec.	10.0_4 km/sec.	13.4_0 km/sec.
U =	13.3_2 km/sec.	17.2_0 km/sec.	21.2_0 km/sec.
U_m =	9.3_0 km/sec.	11.6_1 km/sec.	14.2_5 km/sec.
μ_m =	3.3_0 km/sec.	4.9_6 km/sec.	6.6_1 km/sec.
P =	2.3_8 megabars	4.4_5 megabars	7.4_7 megabars

thermal component of internal energy delivered by shock reaches 1,700 joules in iron when μ_m reaches about 3.1 km/sec. The thermal component of energy rises rapidly, so that the critical value of μ_m is not too sensitive to error in the enthalpy required for fusion. The compression of iron at 3.1 km/sec. μ_m is 0.35_5; from figure 5 the compression of the rocks will be about 0.48_5. Substituting these values along with the adopted initial densities into equation 14, the minimum velocity of impact is given as

$$v = 3.1 \left(1 + \sqrt{\frac{7.85}{2.62} \cdot \frac{0.485}{0.355}} \right) \text{ km/sec.} = 9.4 \text{ km/sec.} \qquad (18)$$

The course of penetration by compression may be illustrated for 15 km/sec. impact velocity using values given in table 1. Consider the meteorite now an infinite plate of thickness $\underline{L}$. At the moment the shock into the meteorite reaches the back side of the plate, 1) the shock into the ground will have penetrated a distance of $(U/U_m)\underline{L}$ or $1.48\,\underline{L}$, 2) the impact interface or leading face of the meteorite will have penetrated $(\mu/U_m)\underline{L}$ or $0.87_4\underline{L}$, 3) the back side of the meteorite will have penetrated $(\mu/U_m + \delta_m - 1)\underline{L}$ or $0.30_0\,\underline{L}$ below the original ground surface, 4) the center of gravity of the compressed system will be $0.78_2\underline{L}$ underground, and 5) the whole compressed system of rock and meteorite will have a velocity of 10.0_4 km/sec. into the ground. This is the moment of greatest compression of the meteorite. The kinetic

energy of the compressed system, given by $\frac{1}{2}\left(1 + \sqrt{\rho_{xo}\,\delta_m / \rho_{mo}\,\delta_x}\right) M\mu^2$, where M is the mass of the meteorite, will be 2/3 of the original kinetic energy of the meteorite ($\frac{1}{2}Mv^2$); the internal energy of the compressed system, given by $\frac{1}{2}MP\left(\delta_m/\rho_{mo} + \delta_x/\rho_{xo}\sqrt{\rho_{xo}\,\delta_m/\rho_{mo}\,\delta_x}\right)$ (see equation 3), will be 1/3 of the original kinetic energy, or $0.37\times10^{12}M$ ergs. About 2/3 of the internal energy will be in the compressed rock and 1/3 in the compressed meteorite and the mean specific internal energy will be 0.25×10^{12} ergs/gm. (The heat of explosion of TNT is conventionally taken as 10^3 cals/gm or $0.041_6 \times 10^{12}$ ergs/gm.) About 53 percent of the total energy will have been transferred from the meteorite to the compressed rock.

When the shock hits the back side of the meteorite a tensional or rarefaction wave will be reflected back into the meteorite. The particle velocity behind the rarefaction wave, relative to the original unshocked meteorite, will be approximately $2\mu_m$ (Walsh and Christian, 1955, p. 1548-1551); the particle velocity, r, relative to the ground, will be given by

$$r \approx v - 2\mu_m = v\left(1 - \frac{2}{1 + \sqrt{\frac{\rho_{mo}\,\delta_x}{\rho_{xo}\,\delta_m}}}\right). \qquad (19)$$

Employing the condition of conservation of momentum, the velocity of the rarefaction into the shocked meteorite relative to the shocked meteorite, U_{mr}, is given by

$$U_{mr} \approx \frac{v\left(\frac{1}{\delta_m} - 1\right)}{\frac{1}{\sqrt{\frac{\rho_{xo}\,\delta_m}{\rho_{mo}\,\delta_x}}} + 1}, \tag{20}$$

and, by the time the rarefaction reaches the impact interface or leading side of the meteorite, the shock into the ground will have engulfed a new increment of rock of mass X_1, given by

$$X_1 = M\left(1 - \frac{r}{\mu}\right). \tag{21}$$

For $v = 15$ km/sec. impact velocity, the particle velocity of the meteorite behind the rarefaction will be about 5.1 km/sec. into the ground.

At the moment the rarefaction reaches the leading face of the meteorite, the shock into the ground will have engulfed a new increment of rock of mass about 0.49M and will have penetrated about 3.0 $\underline{L}$ into the ground. The leading face of the meteorite will have penetrated about 1.8 $\underline{L}$ and the back side about 0.8 $\underline{L}$. The center of gravity of the moving system will be about 1.8 $\underline{L}$ underground. About 88 percent of the original (kinetic) energy of the meteorite will have been transferred to

the compressed rock, where the energy will be divided equally into an internal and a kinetic fraction. The specific internal energy of the compressed rock will be about 0.50×10^{12} ergs/gm or about 12 times the heat of explosion of TNT. The center of gravity of the total energy will be about 2.2 L underground and the compressed rock will be still moving into the ground at 10.0_4 km/sec.

Penetration by hydrodynamic flow. --It is not profitable to carry the the analysis of an infinite plate much further because of the influence of the lateral boundaries of the meteorite in a more realistic case. Rarefaction waves will also be reflected from the sides of an actual meteorite, which will permit lateral flow as well as longitudinal compression. The initial effect of the rarefaction waves reflected from the sides of a meteorite body of more or less equidimensional shape will be to accentuate the flattening by increasing the lateral dimensions of the body as it enters the ground (compare with Öpik, 1958) and to smear out or increase the width of the shock front as it reaches the back end of the meteorite. Lateral flow of the meteorite will decrease somewhat the penetration due to compression in the initial stages of impact, but lateral flow becomes part of the dominant mechanism of penetration as the meteorite and the compressed wad of rock leading the meteorite slow down. The flattening will not significantly alter the initial pressure or transfer of energy from the meteorite to the compressed rock, as calculated above.

Penetration by hydrodynamic flow is brought about by lateral deflection of material at the leading end of the still fast-moving system of compressed rock and meteorite and by sweeping aside of rock newly engulfed by shock along the path of the penetrating body. As the body or slug of fast-moving rock and meteorite is deflected at the leading end, the whole slug is literally turned inside out; the trailing meteorite becomes the liner of a transient cavity, material from the back side of the meteorite facing the center of the cavity (fig. 7, sketches 3 and 4).

Following Rostoker (1953, p. 14), the depth of penetration by lateral deflection of the target rocks may be roughly estimated by treating the initial slug of compressed rock and meteorite as a short jet or column of incompressible fluid. Under the condition that the velocity of the jet is sufficiently high that a hydrodynamic approximation is valid for the target rock, the depth of penetration, D, is given (Birkoff and others, 1948, p. 577) by

$$D \approx J \sqrt{\rho_j / \rho_{xo}} \qquad (22)$$

where J is the length and ρ_j the density of the jet. For the case of 15 km/sec. impact velocity, the jet will be taken as the system of compressed rock and trailing decompressed meteorite at the moment the rarefaction reflected from the back of the meteorite reaches the front of the meteorite. Lateral flow of the meteorite and compressed rock will be neglected up to this point; this error will probably be more than

compensated by further penetration due to compression of rocks in the path of the jet. Treating the system as two successive jets,

$$D \approx J_x \sqrt{\rho_{jx}/\rho_{xo}} + J_m \sqrt{\rho_{jm}/\rho_{xo}} \approx \frac{2\,L\,(U-\mu)}{U_m} \sqrt{\frac{1}{1-\delta_x}} + L\sqrt{\rho_{mo}/\rho_{xo}}, \quad (23)$$

and substituting values from table 1 for 15 km/sec. impact velocity, $D = 3.6\,\underline{L}$. Thus, at the moment the last of the jet or slug is deflected, the bottom of the cavity would be $3.0\,\underline{L}$ (from compression) + $3.6\,\underline{L}$ (from hydrodynamic flow), or $6.6\,\underline{L}$ below ground. The center of gravity of the energy should be roughly 4 to 5 $\underline{L}$ underground.

Dispersal of meteoritic material in the shock wave.--The cavity will continue to expand as the shock is propagated into the rock away from the cavity. All material engulfed by the expanding shock front is imparted an initial velocity more or less in the direction of shock propagation, which will be roughly along the radii of a sphere at distances of several $\underline{L}$ from the center of the cavity. As the shock engulfs an ever-increasing volume of rock the shock strength will decrease; the pressure and internal energy increments across the shock front will decrease roughly as inverse functions of some power of the radius exceeding 3. Beyond the distance where the rock is fused by shock the pressure may be inversely proportional to roughly the sixth or seventh power of the radius (see Porzel, 1958, p. 7). Ultimately the shock becomes an ordinary elastic wave.

Outward motion of material behind the shock will not be uniform, owing to the fact that the pressure soon drops to levels where the strength of the rocks strongly influences the flow. A mixing or scrambling motion occurs in the shock wave permitting fused rock and meteoritic material to be shot out and dispersed in a large volume of rock that is relatively only weakly shocked. Description of breccias formed in this way and the inferred mechanics of mixing will be given in a separate paper (Shoemaker, in preparation). Empirically, the distance from the origin of the shock to the limit of mixing is proportional to the cube root of the total shock energy, and in the nuclear craters is the vertical distance from the device to the lower limit of the breccia under the crater floor. This distance, R, in feet, is given by the empirical equation for alluvium and rocks at the Nevada Test Site (Shoemaker, in preparation) by

$$R = 5.7\ W^{1/3} \qquad (24)$$

where W is the yield or total shock energy in tons of TNT equivalent (1 metric ton TNT = 10^9 calories or 4.16×10^{16} ergs).

Energy, size, and velocity of meteorite.--The initial pressures behind the shocks produced by high velocity impact are comparable to the initial pressures produced by detonation of nuclear devices of yields similar to the devices used at the Teapot Ess and Jangle U craters (compare table 1 with Johnson and Violet, 1958, p. 9). The total shock energy for Meteor

Crater may be estimated by scaling from the structurally similar Teapot Ess crater, employing the empirical Lampson cube root scaling law (Glasstone, 1957, p. 198) for constant scaled depth of explosion

$$d \propto W^{1/3} \tag{25}$$

where d is the diameter of the crater. This scaling relation may be justified dimensionally if it is assumed that the model ratio of pressure is unity. Scaling from craters produced by high explosives will lead to underestimation of the energy for Meteor Crater (compare with Wylie, 1943; and Baldwin, 1949, p. 224) because of the lower initial pressures produced by chemical explosions. At high pressures a significant fraction of the energy is absorbed by fusion of rock.

The ratios of lateral dimensions of Meteor Crater to Teapot Ess crater (fig. 4) are as follows: a) diameter of hinge (intersection of axial plane of overturning with original surface of the ground)--10.5; b) present inside diameter at level of original ground surface--11.2; c) original inside diameter at level of original ground surface--11.4. The corresponding energy ratios from the cube root scaling law are a) 1.16×10^3, b) 1.4×10^3, and c) 1.5×10^3; the indicated total shock energy for Meteor Crater is a) 1.4 megatons, b) 1.7 megatons, and c) 1.8 megatons, respectively (yield for Teapot Ess crater is 1.2 ± 0.05 kilotons). A small positive correction could be added to these estimates for the energy to take account of a scaled depth of apparent shock

origin somewhat shallower than the depth of the device at Teapot Ess crater as indicated below, but the magnitude of the correction would be less than the range of estimates given.

For the minimum possible velocity of 9.4 km/sec. and the maximum indicated energy of 1.8 megatons, the maximum mass of the meteorite (given by $2W/v^2$) is 166,000 metric tons. Taking a more conservative estimate of the total energy of 1.7 megatons and a velocity of 15 km/sec., the mass of the meteorite would be 63,000 tons. The diameter of a sphere of this mass with a density of 7.85 gm/cm^3 would be 24.8 meters or 81 feet. If 80 feet is taken as the length of the meteorite, $\underline{L}$, the center of gravity of the energy released, or apparent origin of the shock, which was estimated at roughly 4 to 5 $\underline{L}$ underground for 15 km/sec. impact velocity, would be 320 to 400 feet from the original surface along the path of penetration. For a total energy of 1.7 megatons, employing equation 24, the apparent origin of the shock should be 680 feet above the lower limit of the breccia under the crater floor or about 400 feet below the original surface (fig. 4). These results are harmonious with the fact that the bulk of the fused rock thrown out is derived from Coconino sandstone, and also with the fact that underthrusting away from the center of the crater has occurred at least as low as the Toroweap-Kaibab contact.

An impact velocity of 15 km/sec. is also consonant with the amount of fine-grained meteoritic material estimated by Rinehart (1958) to be strewn around the crater. From analogy with Teapot Ess crater somewhat less than half of the breccia with dispersed meteoritic material may be expected to be thrown out by the reflected tensional wave. The median concentration of meteoritic material in samples taken by Rinehart from areas I have mapped as Recent alluvium is about 20 percent (with a probable error of a factor of 2) of the median concentration in Pleistocene alluvium. The fine-grained meteoritic material still left around the crater is, of course, strewn out in the downstream direction (cf. fig. 1 and 2 with Rinehart, 1958, fig. 7). If the loss of meteoritic material due to erosion is estimated conservatively as 60 percent, then 30,000 tons may be estimated to have been thrown out, or about half of the 63,000 tons total mass estimated for 15 km/sec. impact velocity.

Finally it may be noticed that the suggested 15 km/sec. impact velocity is within the range and close to the mode of entry velocities computed for observed meteorite falls by Whipple and Hughes (1955, p. 155) and within the range of possible geocentric velocities for known asteroids.

The original shape of the meteorite and its trajectory are not known and probably cannot be determined from the evidence at Meteor Crater alone. It has been suggested that the mass which struck the ground was not a single body but a cluster or shower of individuals (Barringer, 1910,

p. 17-23; Barringer, D. M., Jr., 1927, p. 146; Nininger, 1951b, p. 81-85). It seems likely that individual specimens or fragments surrounding the crater which have undergone no noticeable or only minor impact damage (Nininger, 1950; 1951b, p. 79-82) have landed independently of the mass which formed the crater and were decelerated by atmospheric friction. The preservation of what appears to be parts of surfaces formed by ablation during atmospheric flight on some of these fragments (E. P. Henderson, oral communication, 1959) greatly strengthens this conclusion. In all probability the meteorite was breaking up during its flight through the atmosphere. If the mass which formed the crater consisted of a tight cluster of fragments, the mechanics of penetration would probably not be greatly different than for a single body. It is entirely possible, on the other hand, for fairly large unfused fragments derived from a single body to have been dispersed in the breccia, because a layer on the back side of the meteorite would have escaped maximum shock pressures owing to the smearing out of the shock front by rarefaction waves reflected from the sides. (See evidence for solid fragments in Tilghman, 1905, p. 908-910).

The occurrence of meteorite-bearing breccia under the south rim of the crater is inconclusive evidence, and, in the writer's opinion, exceedingly weak evidence of impact from the north. Similar breccia may occur under any part of the rest of the rim. This breccia may have been

injected along transient bedding-plane fissures opened up by shock or possibly by the tensional wave reflected from the ground surface. Such transient bedding-plane openings were formed in experiments with underground detonation of 10 and 50 tons of dynamite at the Nevada Test Site (Cattermole, written communication, 1959; Hansen and Lemke, 1959). The relatively good agreement between semi-independent lines of evidence for the depth of the apparent origin of the shock suggests the zenith angle of impact was small, but many combinations of elongation of the meteorite and angle of impact would fit the analysis equally well.

The sequence of events in the formation of Meteor Crater, Arizona, as here conceived, is summarized schematically in figure 7. In the

---

Figure 7. Diagrammatic sketches showing sequence of events in formation of Meteor Crater, Arizona.

---

final stages of crater formation it will be noted that the breccia under the crater floor changes shape slightly due to slumping. This slumping may be demonstrated by major downward displacement of Kaibab block-bearing breccia against the Coconino sandstone along the walls of the crater; it appears to have preceded the showering down of the mixed debris. Modification by erosion and by deposition of sediments has produced the crater we see today. The surface morphology of large meteorite craters should not be compared uncritically with experimental models.

1. Meteorite approaches ground at 15 km/sec.

2. Meteorite enters ground, compressing and fusing rocks ahead and flattening by compression and by lateral flow. Shock into meteorite reaches back side of meteorite.

3. Rarefaction wave is reflected back through meteorite, and meteorite is decompressed, but still moves at about 5 km/sec into ground. Most of energy has been transferred to compressed fused rock ahead of meteorite.

4. Compressed slug of fused rock and trailing meteorite are deflected laterally along the path of penetration. Meteorite becomes liner of transient cavity.

5. Shock propogates away from cavity, cavity expands, and fused and strongly shocked rock and meteoritic material are shot out in the moving mass behind the shock front.

6. Shell of breccia with mixed fragments and dispersed fused rock and meteoritic material is formed around cavity. Shock is reflected as rarefaction wave from surface of ground and momentum is trapped in material above cavity.

7. Shock and reflected rarefaction reach limit at which beds will be overturned. Material behind rarefaction is thrown out along ballistic trajectories.

8. Fragments thrown out of crater maintain approximate relative positions except for material thrown to great height. Shell of breccia with mixed meteoritic material and fused rock is sheared out along walls of crater; upper part of mixed breccia is ejected.

9. Fragments thrown out along low trajectories land and become stacked in an order inverted from the order in which they were ejected. Mixed breccia along walls of crater slumps back toward center of crater. Fragments thrown to great height shower down to form layer of mixed debris.

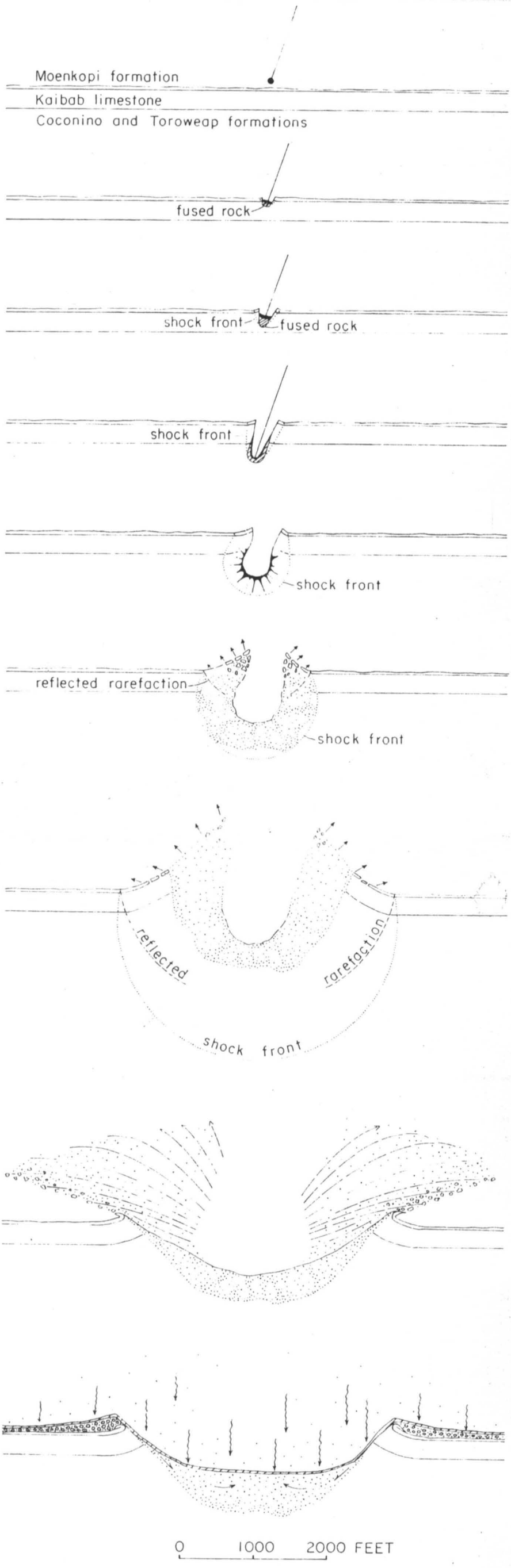

FIGURE 7. DIAGRAMATIC SKETCHES SHOWING SEQUENCE OF EVENTS IN FORMATION OF METEOR CRATER, ARIZONA

Acknowledgments

It is a pleasure to acknowledge the wholehearted cooperation of the Barringer Crater Company, whose officers not only permitted full access to all parts of the crater, but also gave encouragement during the course of this research and material support in underground investigations in shafts in the floor of the crater. To Mr. D. Moreau Barringer, Jr., president of the company, to Mr. E. W. Chilson, president of Meteor Crater Enterprises, Inc., and to Mr. George E. Foster, curator of the museum at the crater, I owe special thanks for many courtesies extended while in the field. This work was supported by the Research Division of the Atomic Energy Commission.

References cited

Altshuler, L. V., Krupnikov, K. K., Ledenev, B. N., Zhuchikhin, V. I. and Brazhnik, M. I., 1958, Dynamical compressibility and equation of state for iron under high pressure (in Russian): Jour. Experimental and Theoretical Physics, p. 874-885; English translation in Soviet Physics JETP, v. 7, p. 606-614, 1958.

Baldwin, R. B., 1949, The face of the moon: Chicago, Ill., Chicago Univ. Press, 239 p.

Bancroft, Dennison, Peterson, E. L., and Minshall, S. F., 1956, Polymorphism of iron at high pressure: Jour. Appl. Physics, v. 27, p. 291-298.

Barringer, D. M., 1905, Coon Mountain and its crater: Acad. Nat. Sciences Philadelphia Proc., v. 57, p. 861-886.

____1910, Meteor Crater (formerly called Coon Mountain or Coon Butte) in northern central Arizona: Published by the author, 24 p.

____1914, Further notes on Meteor Crater, Arizona: Acad. Nat. Sciences Philadelphia Proc., v. 66, p. 556-565.

____1924, Further notes on Meteor Crater in northern central Arizona (No. 2): Acad. Nat. Sciences Philadelphia Proc., v. 76, p. 275-278.

Barringer, D. M., Jr., 1927, The most fascinating spot on earth /Meteor Crater, Arizona/: Sci. Am., v. 137, p. 52-54, 144-146, 244-246.

Birch, Francis, 1947, Finite elastic strain of cubic crystals: Phys. Rev., v. 71, p. 809-824.

____1952, Elasticity and constitution of the earth's interior: Jour. Geophys. Research, v. 57, p. 227-286.

Birkhoff, Garret, MacDougall, D. P., Pugh, E. M., and Taylor, Sir Geoffrey, 1948, Explosives with lined cavities: Jour. Appl. Physics, v. 19, p. 563-581.

Boon, J. D., 1936, The impact of meteors: Field and Lab., v. 4, p. 56-59.

Boon, J. D., and Albritton, C. C., Jr., 1936, Meteorite craters and their possible relations to "cryptovolcanic structures": Field and Lab., v. 5, p. 1-9.

____1937, Meteorite scars in ancient rocks: Field and Lab., v. 5, p. 53-64.

____1938, The impact of large meteorites: Field and Lab., v. 6, p. 57-64.

Bridgman, P. W., 1928, The linear compressibility of thirteen natural crystals: Am. Jour. Sci., 5th ser., v. 15, p. 287-296.

____1939, The high pressure behavior of miscellaneous minerals: Am. Jour. Sci., n. s., v. 237, p. 7-18.

____1948a, The compression of 39 substances to 100,000 Kg/cm^2: Am. Acad. Arts and Sci. Proc., v. 76, p. 55-70.

____1948b, Rough compressions of 177 substances to 40,000 Kg/cm^2: Am. Acad. Arts and Sci. Proc., v. 76, p. 71-87.

Bridgman, P. W., 1949, Linear compressions to 30,000 Kg/cm^2, including relatively incompressible substances: Am. Acad. Arts and Sci. Proc., v. 77, p. 187-234.

Bullen, K. E., 1940, The problem of the earth's density variation: Seismol. Soc. America Bull., v. 30, p. 235-250.

_____1942, The density variation of the earth's central core: Seismol. Soc. America Bull., v. 32, p. 19-29.

_____1946, A hypothesis on compressibility at pressures of the order of a million atmospheres: Nature, v. 157, p. 405.

_____1949, Compressibility-pressure hypothesis and the earth's interior: Royal Astron. Soc. Monthly Notices, Geophys. Supp., v. 5, p. 355-368.

_____1950, An earth model based on a compressibility-pressure hypothesis: Royal Astron. Soc. Monthly Notices, Geophys. Supp., v. 6, p. 50-59.

_____1952, On density and compressibility at pressures up to thirty million atmospheres: Royal Astron. Soc. Monthly Notices, Geophys. Supp., v. 6, p. 383-401.

_____1956, Seismology and the broad structure of the earth's interior, in Physics and Chemistry of the Earth: New York, McGraw-Hill Book Co., Inc., p. 68-93.

Courant, Richard, and Friedrichs, K. O., 1948, Supersonic flow and shock waves: New York, Interscience Publishers, Inc., 464 p.

Darton, N. H., 1916, Explosion craters: Sci. Monthly, v. 3, p. 417-430.

_____1945, Crater Mound, Ariz. (abs.): Geol. Soc. America Bull., v. 56, p. 1154.

Du Mond, J. W. M., and Cohen, E. R., 1952, Recent advances in our knowledge of the numerical values of the fundamental atomic constants: Am. Scientist, v. 40, p. 447-467.

Elsasser, W. M., 1951, Quantum-theoretical densities of solids at extreme compression: Science, n. s., v. 113, p. 105-107.

Fairchild, H. L., 1930, Nature and fate of the Meteor Crater bolide: Science, v. 72, p. 463-467.

Feynman, R. P., Metropolis, N. C., and Teller, Edward, 1949, Equations of state of elements based on the generalized Fermi-Thomas theory: Phys. Rev., v. 75, p. 1561-1573.

Foster, G. E., 1957, The Barringer (Arizona) meteorite crater: Meteor Crater, Arizona, 31 p.

Gifford, A. C., 1924, The mountains of the moon: New Zealand Jour. Sci. and Technology, v. 7, p. 129-142.

_____1930, The origin of the surface features of the moon: New Zealand Jour. Sci. and Technology, v. 11, p. 319-327.

Gilbert, G. K., 1896, The origin of hypotheses, illustrated by the discussion of a topographic problem: Science, n. s., v. 3, p. 1-13.

Gilvarry, J. J., and Hill, J. E., 1956a, The impact theory of the origin of lunar craters: Pub. Astron. Soc. of the Pacific, v. 68, p. 223-229.

Gilvarry, J. J., and Hill, J. E., 1956b, The impact of large meteorites: Astrophys. Jour., v. 124, p. 610-622.

Glasstone, Samuel (ed.), 1957, The effects of nuclear weapons: Washington, D. C., U. S. Atomic Energy Commission, 579 p.

Gold, Thomas, 1956, The lunar surface: Royal Astron. Soc. Monthly Notices, v. 115, p. 585-604.

Goranson, R. W., and others, 1955, Dynamic determination of the compressibility of metals: Jour. Appl. Physics, v. 26, p. 1472-1479.

Hack, J. T., 1942, The changing physical environment of the Hopi Indians: Peabody Mus. Nat. History Papers, v. 35, p. 3-85.

Hager, Dorsey, 1953, Crater Mound (Meteor Crater), Arizona, a geologic feature: Am. Assoc. Petroleum Geologists Bull., v. 37, p. 821-857.

Hansen, W. R., and Lemke, R. W., 1959, Geology of the U.S.G.S. and Rainier Tunnel areas, Nevada Test Site: U. S. Geol. Survey open-file report, 111 p.

Hardy, C. T., 1953, Structural dissimilarity of Meteor Crater and Odessa meteorite crater: Am. Assoc. Petroleum Geologists Bull., v. 37, p. 2580.

Hill, J. E., and Gilvarry, J. J., 1956, Application of the Baldwin crater relation to the scaling of explosion craters: Jour. Geophys. Research, v. 61, p. 501-511.

Hughes, D. S., and McQueen, R. C., 1958, Density of basic rocks at very high pressures: Am. Geophys. Union Trans., v. 39, p. 959-965.

Jakosky, J. J., Wilson, C. H., and Daly, J. W., 1932, Geophysical examination of Meteor Crater, Arizona: Am. Inst. Mining Metall. Eng., Geophys. Prospecting, p. 1-35.

Johnson, G. W., 1959, Mineral resource development by the use of nuclear explosives: California Univ., Lawrence Radiation Lab. Rept. 5458, 18 p.

Johnson, G. W., and Violet, C. E., 1958, Phenomenology of contained nuclear explosions: California Univ., Lawrence Radiation Lab. Rept. 5124, Rev. 1, 27 p.

Knopoff, Leon, and Uffen, R. J., 1954, The densities of compounds at high pressures and the state of the earth's interior: Jour. Geophys. Research, v. 59, p. 471-484.

Leopold, L. B., and Miller, J. P., 1954, A post-glacial chronology for some alluvial valleys in Wyoming: U. S. Geol. Survey Water-Supply Paper 1261, 90 p.

McKee, E. D., 1934, The Coconino sandstone--its history and origin: Carnegie Inst. Washington Pub. 440, p. 77-115.

_____1938, The environment and history of the Toroweap and Kaibab formations of northern Arizona and southern Utah: Carnegie Inst. Washington Pub. 492, 268 p.

McKee, E. D., 1954, Stratigraphy and history of the Moenkopi formation of Triassic age: Geol. Soc. America Mem. 61, 133 p.

Madelung, Erwin, and Fuchs, R., 1921, Compressibility measurements on solid bodies: Annalen der Physik, v. 65, no. 4, p. 289-309.

March, N. H., 1957, The Thomas-Fermi approximation in quantum mechanics: Advances in Physics, v. 6, p. 1-101.

Merrill, G. P., 1907, On a peculiar form of metamorphism in siliceous sandstone: U. S. Natl. Mus. Proc., v. 32, p. 547-550.

_____1908, The meteor crater of Canyon Diablo, Arizona; its history, origin, and associated meteoritic irons: Smithsonian Inst. Misc. Coll., v. 50, p. 461-498.

Merrill, G. P., and Tassin, Wirt, 1907, Contributions to the study of the Canyon Diablo meteorites: Smithsonian Inst. Misc. Coll., v. 50, p. 203-214.

Metropolis, N. C., and Reitz, J. R., 1951, Solutions of the Fermi-Thomas-Dirac equation: Jour. Appl. Physics, v. 19, p. 555-573.

Meyerhoff, Howard, 1950, Meeting of the Southwestern Division of the AAAS: Science, v. 111, p. 679-680.

Moulton, F. R., 1931, Astronomy: New York, The Macmillan Co., 549 p.

Murnaghan, F. D., 1937, Finite deformations of an elastic solid: Am. Jour. Math., v. 59, p. 235-260.

Nininger, H. H., 1949, Oxidation studies at Barringer crater. Metal-center pellets and oxide droplets: Am. Philos. Soc. Yearbook, 1949, p. 126-130.

_____1950, Structure and composition of Canyon Diablo meteorites as related to zonal distribution of fragments: Pop. Astronomy, v. 58, p. 169-173.

_____1951a, Condensation globules at Meteor Crater: Science, v. 113, p. 755-756.

_____1951b, A resume of researches at the Arizona meteorite crater: Sci. Monthly, v. 72, p. 75-86.

_____1954, Impactite slag at Barringer crater: Am. Jour. Sci., v. 252, p. 277-290.

_____1956, Arizona's meteorite crater: Denver, Colo., World Press, Inc.

Öpik, E. J., 1936, Researches on the physical theory of meteor phenomena: Acta et Comm. Univ. Tartu, A 30; Tartu Obs. Publ. 28, p. 1-27.

_____1958, Meteor impact on solid surface: Irish Astron. Jour., v. 5, p. 14-33.

Peirce, H. W., 1958, Permian sedimentary rocks of the Black Mesa basin area: New Mexico Geol. Soc. 9th Field Conference, Guidebook of the Black Mesa Basin, Northeastern Arizona, p. 82-87.

Porzel, F. B., 1958, A new approach to heat and power generation from contained nuclear explosions: Second United Nations International Conference on the Peaceful Uses of Atomic Energy, A/CONF./P/2178, 13 p.

Ramsey, W. H., 1948, On the constitution of the terrestrial planets: Royal Astron. Soc. Monthly Notices, v. 108, p. 406-413.

Rogers, A. F., 1928, Natural history of the silica minerals: Am. Mineralogist, v. 13, p. 73-92.

Rogers, A. F., 1930, A unique occurrence of lechatelierite or silica glass: Am. Jour. Sci., 5th ser., v. 19, p. 195-202.

Rinehart, J. S., 1950, Some observations on high-speed impact: Contributions of the Meteoritical Society, v. 4, p. 299-305; also in Pop. Astronomy, v. 66, p. 458-464.

____1958, Distribution of meteoritic debris about the Arizona meteorite crater: Smithsonian Inst. Contrib. Astrophys., v. 2, p. 145-160.

Rostoker, Norman, 1953, The formation of craters by high-speed particles: Meteoritics, v. 1, p. 11-27.

Sellards, E. H., and Evans, G. L., 1941, Statement of progress of investigation at Odessa meteor craters: Texas Univ., Bur. Econ. Geology, 13 p.

Shoemaker, E. M., 1956, Occurrence of uranium in diatremes on the Navajo and Hopi Reservations, Arizona, New Mexico, and Utah: in Page, L. R., Stocking, H. E., and Smith, H. B., Contributions to the geology of uranium and thorium by the United States Geological Survey and Atomic Energy Commission for the United Nations International Conference on Peaceful Uses of Atomic Energy, Geneva, Switzerland, 1955: U. S. Geol. Survey Prof. Paper 300, p. 179-185.

Shoemaker, E. M., 1957, Primary structures of maar rims and their bearing on the origin of Kilbourne Hole and Zuni Salt Lake, New Mexico (abs.): Geol. Soc. America Bull., v. 68, no. 12, pt. 2, p. 1846.

Shoemaker, E. M., Byers, F. M., Jr., and Roach, C. H., in press, Diatremes and Cenozoic geology of the Hopi Buttes region, Arizona: Am. Jour. Sci.

Shoemaker, E. M., and Moore, H. J., 2d, 1956, Diatremes on the Navajo and Hopi Reservations, in Geologic investigations of radioactive deposits--Semiannual progress report: U. S. Geol. Survey TEIR-640, p. 197-203, issued by U. S. Atomic Energy Comm. Tech. Inf. Service, Oak Ridge, Tenn.

Slater, J. C., and Krutter, H. M., 1935, The Thomas-Fermi method for metals: Phys. Rev., v. 47, p. 559-568.

Spencer, L. J., 1933, Meteoric iron and silica-glass from the meteorite craters of Henbury (central Australia) and Wabar (Arabia): Mineralog. Mag., v. 23, p. 387-404.

_____1935, Meteorite craters as topographical features on the earth's surface: Smithsonian Inst. Ann. Rept., 1933, p. 307-326.

Strong, H. M., 1959, The experimental fusion curve of iron to 96,000 atmospheres: Jour. Geophys. Research, v. 64, p. 653-659.

Tilghman, B. C., 1905, Coon Butte, Arizona: Acad. Nat. Sciences Philadelphia Proc., v. 57, p. 887-914.

Verhoogen, John, 1953, Elasticity of olivine and constitution of the earth's mantle: Jour. Geophys. Research, v. 58, p. 337-346.

Walsh, J. M., and Christian, R. H., 1955, Equation of state of metals from shock-wave measurements: Phys. Rev., v. 97, p. 1544-1566.

Walsh, J. M., Rice, H. H., McQueen, R. G., and Yarger, F. L., 1957, Shock wave compressions of twenty-seven metals; the equations of state of metals: Phys. Rev., v. 108, p. 196-216.

Whipple, F. L., and Hughes, R. F., 1955, On the velocities and orbits of meteors, fireballs and meteorites: Jour. Atmospheric and Terrestrial Physics, Supp. 2, p. 149-156.

Wylie, C. C., 1933, On the formation of meteoric craters: Pop. Astronomy, v. 41, p. 211-214.

____1934, Meteoric craters, meteors, and bullets: Pop. Astronomy, v. 42, p. 469-471.

____1943, Calculations on the probable mass of the object which formed Meteor Crater: Pop. Astronomy, v. 51, p. 97-99.